# Effective-range dependence of two-dimensional Fermi gases

L. M. Schonenberg, P. C. Verpoort, and G. J. Conduit
*Cavendish Laboratory, J.J. Thomson Avenue, Cambridge CB3 0HE, United Kingdom*
(Received 13 April 2017; published 22 August 2017)

The Feshbach resonance provides precise control over the scattering length and effective range of interactions between ultracold atoms. We propose the ultratransferable pseudopotential to model effective interaction ranges $-1.5 \leqslant k_F^2 R_{\rm eff}^2 \leqslant 0$, where $R_{\rm eff}$ is the effective range and $k_F$ is the Fermi wave vector, describing narrow to broad Feshbach resonances. We develop a mean-field treatment and exploit the pseudopotential to perform a variational and diffusion Monte Carlo study of the ground state of the two-dimensional Fermi gas, reporting on the ground-state energy, contact, condensate fraction, momentum distribution, and pair-correlation functions as a function of the effective interaction range across the BEC-BCS crossover. The limit $k_F^2 R_{\rm eff}^2 \to -\infty$ is a gas of bosons with zero binding energy, whereas $\ln(k_F a) \to -\infty$ corresponds to noninteracting bosons with infinite binding energy.

DOI: 10.1103/PhysRevA.96.023619

## I. INTRODUCTION

Many discoveries in modern condensed-matter physics have emerged in two-dimensional (2D) systems, such as the quantum Hall effect [1], the BKT transition [2], and high-temperature superconductivity [3]. Recent experimental advances allow for the realization of a two-dimensional ultracold atomic gas by means of an anisotropic optical trap that confines one dimension more tightly than the other two [4,5]. In combination with the Feshbach resonance [6,7] this provides a platform for the controlled study of interactions in the two-dimensional Fermi gas, which has attracted considerable interest both experimentally [8–12] and theoretically [12–18] for contact interactions. Here we study the BEC-BCS crossover as a function of the effective range of the interaction.

The scattering of two interacting atoms at low energies is described by the $s$-wave scattering phase shift $\delta(k)$, which up to second order in the wave vector $k$ is parameterized by [19,20],

$$\cot[\delta(k)] = \frac{2}{\pi}\ln(ka) + \frac{k^2 R_{\rm eff}^2}{4}. \tag{1}$$

Here $a$ is the scattering length and $R_{\rm eff}$ the effective range. The noninteracting gas has infinite scattering length, $a = \infty$, and the contact interaction used in earlier theoretical works [21–23] is recovered in the limit of zero effective range, $R_{\rm eff}^2 = 0$. The effective range for a 2D resonance is shown to be related to the 3D effective range by $k_F^2 R_{\rm eff}^2 \simeq k_F^2 l_z R_{\rm eff}^{\rm 3D}$, with Fermi wave vector $k_F$ and the harmonic oscillator length of the tight confinement direction is $l_z$. $R_{\rm eff}^{\rm 3D} < 0$ for narrow Feshbach resonances and $R_{\rm eff}^{\rm 3D} \approx 0$ for broad Feshbach resonances so that in typical experiments exploiting the full gamut of available resonances, $-100 \lesssim k_F^2 R_{\rm eff}^2 \lesssim 0$ [6,12,24].

In this paper, we extend the analysis of Refs. [25,26] to derive a mean-field theory that is quantitatively correct in the limit of large negative effective interaction range $k_F^2 R_{\rm eff}^2 \ll -1$. This is complemented by variational Monte Carlo (VMC) and diffusion Monte Carlo (DMC) simulations in the strongly interacting regime, for which we develop an ultratransferable pseudopotential (UTP) following Refs. [27–30] that is calibrated to deliver both the correct scattering phase shift and correct binding energy for the two-body bound state for $-1.5 \leqslant k_F^2 R_{\rm eff}^2 \leqslant 0$. Exploiting the UTP, we first revisit the case $R_{\rm eff}^2 = 0$ [21–23], which we next use as a concrete basis to analyze $R_{\rm eff}^2 < 0$ by considering the ground-state energy, condensate fraction, momentum distribution, and pair-correlation functions.

In Sec. II we study the two-body problem and use it as a building block for our mean-field theory of the many-body problem. In Sec. III we propose the UTP and demonstrate that its scattering phase shift and bound-state energy are more accurate than the conventional potential well. We study how the BEC-BCS crossover evolves as a function of the effective interaction range using DMC in Sec. IV. Finally, we provide a discussion of our main findings in Sec. V.

## II. MEAN-FIELD THEORY

We develop a mean-field theory for the ground state to provide a solid foundation for our investigations. The theory becomes exact in the noninteracting limit, $R_{\rm eff}^2 \to -\infty$. For less negative values of $R_{\rm eff}^2$ fluctuations around the mean-field solution increase and the mean-field theory remains qualitatively correct, but serves as a concrete base to compare with our quantum Monte Carlo study of the strongly interacting regime. Our two-dimensional treatment is analogous to the three-dimensional case discussed in Ref. [31].

We use the two-channel model introduced in Ref. [32] and employ atomic units ($\hbar = m = 1$) throughout this text,

$$\hat{H}^{2-\rm ch} = \sum_{\mathbf{k},\sigma} \frac{k^2}{2} c_{\mathbf{k}\sigma}^\dagger c_{\mathbf{k}\sigma} + \sum_{\mathbf{p}} \left(\epsilon_0 + \frac{p^2}{4}\right) b_{\mathbf{p}}^\dagger b_{\mathbf{p}} + \sum_{\mathbf{k},\mathbf{p}} \frac{\lambda}{\sqrt{A}} \left(b_{\mathbf{p}} c_{\frac{\mathbf{p}}{2}+\mathbf{k}\uparrow}^\dagger c_{\frac{\mathbf{p}}{2}-\mathbf{k}\downarrow}^\dagger + \text{H.c.}\right). \tag{2}$$

$c_{\mathbf{k}\sigma}^\dagger$ creates and $c_{\mathbf{k}\sigma}$ annihilates a fermion with momentum $\mathbf{k}$ and spin $\sigma$ respectively. Similarly, $b_{\mathbf{p}}^\dagger$ creates and $b_{\mathbf{p}}$ annihilates a boson with momentum $\mathbf{p}$. $\epsilon_0$ is the bare detuning of the bosonic mode, $\lambda$ is the coupling between the fermionic and bosonic channels, and $A$ is the area.

 

We first solve exactly for the two-body sector in this theory, relating the model parameters $\lambda$ and $\epsilon_0$ to the physical scattering length $a$ and effective range $R_{\text{eff}}$. We then study the many-body problem in mean-field approximation, computing the chemical potential, BCS energy gap, and ground-state energy.

### A. Two-body problem

To calibrate the model parameters $\lambda$ and $\epsilon_0$, we compute the two-body scattering amplitude using the two-channel model Hamiltonian, and match the result to the scattering amplitude corresponding to the desired scattering phase shift. We consider the scattering of a spin-up fermion with momentum $\mathbf{p}/2+\mathbf{k}$ and a spin-down fermion with momentum $\mathbf{p}/2-\mathbf{k}$, so that the center-of-mass momentum is $\mathbf{p}$, while the momentum in the center-of-mass frame is $\mathbf{k}$. The scattering amplitude $f$ equals to the $T$ matrix [33], which is computed as the renormalized four-point vertex, $T(\mathbf{k},\mathbf{k}')=\Gamma(\mathbf{p}/2+\mathbf{k},\mathbf{p}/2-\mathbf{k},\mathbf{p}/2+\mathbf{k}',\mathbf{p}/2-\mathbf{k}')$. As the contact interaction has no angular dependence, we expect only $s$-wave scattering so that the $T$ matrix depends only on the magnitude of the relative momentum $k=|\mathbf{k}|=|\mathbf{k}'|$.

The $T$ matrix is computed as the sum of the geometric perturbation series in $\lambda$,

$$T(k)=[(\lambda^2 D_0)^{-1}-\Pi]^{-1}. \tag{3}$$

$D_0$ is the bosonic propagator evaluated at momentum $\mathbf{p}$ and energy $k^2+p^2/4$, and $\Pi$ is the polarization operator for fermions with relative energy $k^2$,

$$D_0^{-1}=k^2-\epsilon_0+i0^+, \tag{4}$$

$$\Pi=-\frac{1}{4\pi}\ln\left(1-\frac{2\Lambda^2}{k^2}\right). \tag{5}$$

$0^+$ is an infinitesimal positive number and $\Lambda$ is a momentum cutoff, required to regularize the integral over the relative momentum of the two particles that diverges as the result of the contact interaction between the fermionic and bosonic channels. Physically, the regularization leads to a renormalization of the bare detuning $\epsilon_0$ to give a physical detuning $\omega_0$,

$$\omega_0=\epsilon_0-\frac{\lambda^2}{2\pi}\ln(\Lambda/q^*), \tag{6}$$

where $q^*$ is an arbitrary momentum scale that can be chosen at convenience.

Assuming the momentum cutoff to be arbitrarily large, $\Lambda\gg k$, the scattering amplitude reads,

$$f(k)=\frac{4}{-\frac{2}{\pi}\ln\left(\frac{k}{q^*}e^{2\pi\omega_0/\lambda^2}\right)+\frac{4k^2}{\lambda^2}+i}. \tag{7}$$

The scattering amplitude is related to the phase shift as $f(k)=4/\{\cot[\delta(k)]-i\}$ [33], so in terms of the scattering length $a$ and effective range $R_{\text{eff}}$

$$f(k)=\frac{4}{-\frac{2}{\pi}\ln(ka)-\frac{k^2R_{\text{eff}}^2}{4}+i}. \tag{8}$$

Matching both expressions, we can express $\omega_0$ and $\lambda$ in terms of $a$ and $R_{\text{eff}}$,

$$\omega_0=-\frac{8}{\pi R_{\text{eff}}^2}\ln(q^*a), \tag{9a}$$

$$\lambda^2=-\left(\frac{4}{R_{\text{eff}}}\right)^2. \tag{9b}$$

The 2D scattering length $a$ and effective range $R_{\text{eff}}$ are related to their 3D counterparts $a^{3D}$ and $R_{\text{eff}}^{3D}$ through the physical detuning, which is independent of dimensionality and related to the experimental magnetic field. Equating the 3D detuning $2/(R_{\text{eff}}^{3D}a^{3D})$ [31] to the 2D detuning, (9a),

$$a=(q^*)^{-1}\exp\left[-4R_{\text{eff}}^2/\left(\pi a^{3D}R_{\text{eff}}^{3D}\right)\right]. \tag{10}$$

This expression is of the same form as the one found by Petrov and Shlyapnikov [34] for particles confined to a two-dimensional plane by a harmonic potential, $a\simeq 1.86\,l_z\exp(-\sqrt{\pi/2}l_z/a^{3D})$, where the harmonic oscillator length in the direction normal to the plane $l_z=1/\sqrt{\omega_z}$ with $\omega_z$ the oscillator frequency. Comparing both expressions, we find for the 2D effective range of particles confined in a harmonic potential

$$R_{\text{eff}}^2\simeq 0.984\,l_z R_{\text{eff}}^{3D}. \tag{11}$$

Since $R_{\text{eff}}^{3D}<0$ in experiments, the quantity $R_{\text{eff}}^2$ is also negative.

The energy of the two-body bound state of a pair of fermions, i.e., the renormalized boson, $E_b=k^2$ can be computed from the corresponding pole in the scattering amplitude as

$$E_b=\frac{4}{\pi R_{\text{eff}}^2}W_0\left(-\frac{\pi R_{\text{eff}}^2}{4a^2}\right), \tag{12}$$

where $W_0$ is the principle branch of the Lambert-$W$ function, defined as the solutions to the equation $z=W(ze^z)$. In the limit $R_{\text{eff}}^2\to 0$ the equation reduces to [35], and in the limit $R_{\text{eff}}^2\to-\infty$, $E_b=0$.

As is evident from Eq. (9b), $R_{\text{eff}}^2\to-\infty$ corresponds to the limit $\lambda\to 0$ where the fermions do not interact with the bosons. In this case the two-body bound state of a pair of fermions with energy $E_b=0$ is equal to a bare boson with energy equal to its bare detuning and indeed $\epsilon_0=\omega_0=0$. In the presence of interactions the two-body bound state is a quasiparticle formed of a boson dressed by fermionic fluctuations and its energy is therefore no longer equal to the energy of a bare boson.

### B. Many-body theory

Now that we have calibrated our model parameters to give the desired two-body scattering properties, we turn to the many-particle theory using the noninteracting limit $\lambda\to 0$ as a solid platform. The energy of a boson is zero in this limit, but the energy of a fermion is positive because it has a finite kinetic energy due to the Pauli exclusion principle. The ground state is therefore a BEC of bosons that have no residual interactions with each other, which we shall use as a concrete platform for the development of a perturbative mean-field theory.

We consider the grand-canonical partition function expressed as a path integral. After integrating out the quadratic fermion fields, the partition function becomes $\mathcal{Z} = \int \mathcal{D}\phi\mathcal{D}\bar{\phi}\, \exp(-S[\phi,\bar{\phi}])$, where the action,

$$S[\phi,\bar{\phi}] = \int_0^\beta d\tau \int d^2r \bar{\phi}\left(\partial_\tau + \epsilon_0 - 2\mu - \frac{\nabla^2}{4m}\right)\phi - \ln\det\begin{pmatrix} \partial_\tau - \frac{\nabla^2}{2m} - \mu & \lambda\phi \\ \lambda\bar{\phi} & \partial_\tau + \frac{\nabla^2}{2m} + \mu \end{pmatrix}, \quad (13)$$

is a function of the bosonic field $\phi(\mathbf{r},\tau)$. The imaginary time integral runs up to the inverse temperature $\beta = 1/T$ and $\mu$ is the chemical potential. Since two fermionic particles can convert into a bosonic molecule through the interaction term $\lambda$, $\mu$ couples to the total conserved particle density $n = n_\mathrm{f} + 2n_\mathrm{b}$ where $n_\mathrm{f}$ and $n_\mathrm{b}$ is the density of fermionic and bosonic particles respectively.

We use a mean-field approximation, replacing the path integral over the bosonic field by a single real mean-field $\phi(\mathbf{r},\tau) = B$ that minimizes the action. At zero temperature the BCS equation, obtained from the condition $\delta S/\delta\phi = 0$, and the number equation, obtained as $n = -(T/A)\partial S[B]/\partial\mu$, where the action is now a functional of the mean-field $B$, read,

$$\epsilon_0 - 2\mu = \frac{\lambda^2}{2}\int \frac{d^2k}{(2\pi)^2}\frac{1}{E(k)}, \quad (14a)$$

$$n = 2\left(\frac{\Delta}{\lambda}\right)^2 + \int \frac{d^2k}{(2\pi)^2}\left(1 - \frac{\xi(k)}{E(k)}\right). \quad (14b)$$

With $\Delta = \lambda B$ and the usual BCS expressions for $\xi(k)$ and $E(k)$,

$$\xi(k) = \frac{k^2}{2} - \mu, \quad (15a)$$

$$E(k) = \sqrt{\xi^2(k) + \Delta^2}. \quad (15b)$$

The momentum integral in the gap equation diverges and is regularized as done before by introducing the momentum cutoff $\Lambda$ and eliminating the bare detuning $\epsilon_0$ in favor of the physical detuning $\omega_0$

$$\omega_0 - 2\mu = \frac{\lambda^2}{2}\int \frac{d^2k}{(2\pi)^2}\left[\frac{1}{E(k)} - \frac{2}{k^2}\Theta\left(\frac{k^2}{k_\mathrm{F}^2} - 1\right)\right], \quad (16)$$

where we set $q^* = k_\mathrm{F}$, the Fermi momentum.

The integrals can be performed analytically in terms of the dimensionless ratio $\mu/\Delta$ to obtain our result for $\Delta$ and $\mu$,

$$\omega_0 - 2\mu = \frac{\lambda^2}{4\pi}\left[\operatorname{arcsinh}\left(\frac{\mu}{\Delta}\right) + \ln\left(\frac{k_\mathrm{F}^2}{\Delta}\right)\right], \quad (17a)$$

$$n = 2\left(\frac{\Delta}{\lambda}\right)^2 + \frac{1}{2\pi}[\sqrt{\Delta^2 + \mu^2} + \mu]. \quad (17b)$$

The ground-state grand-canonical potential is then computed as $\lim_{T\to 0} TS[B]/A$. Converting from energy per unit area to energy per particle and adding back the chemical potential, the ground-state energy per particle is

$$E = \frac{2\pi\Delta^2}{k_\mathrm{F}^2\lambda^2}(\omega_0 - 2\mu) - \frac{1}{2k_\mathrm{F}^2}(\mu^2 + \sqrt{\Delta^2 + \mu^2}) - \frac{\Delta^2}{2k_\mathrm{F}^2}\left[\operatorname{arcsinh}\left(\frac{\mu}{\Delta}\right) + \frac{1}{2} + \ln\left(\frac{k_\mathrm{F}^2}{\Delta}\right)\right] + \mu. \quad (18)$$

The BCS equations can be solved analytically in the limit of small $\Delta$, described in Appendix A, and at the BEC-BCS crossover point $\mu = 0$ [17], in which we are interested here. After setting $\mu = 0$ and eliminating $\lambda$ in favor of $R_\mathrm{eff}$, the gap and number equations reduce to

$$\omega_0 = -\frac{4}{\pi R_\mathrm{eff}^2}\ln\left(\frac{k_\mathrm{F}^2}{\Delta}\right), \quad (19a)$$

$$\Delta = \frac{2}{\pi R_\mathrm{eff}^2}[1 - \sqrt{1 - \pi(k_\mathrm{F}R_\mathrm{eff})^2}]. \quad (19b)$$

This shows that $\Delta \to 0$ when approaching the noninteracting limit $R_\mathrm{eff}^2 \to -\infty$ as expected. Furthermore in this limit, the density of the bosons $n_b = B^2 \to n/2$, confirming that all particles convert into composite bosons. Combining Eqs. (19a) and (19b) with Eq. (9a), the scattering length at the crossover point, $\mu = 0$, is related to the effective range as

$$a = \sqrt{\pi/2}|R_\mathrm{eff}|[\sqrt{1 - \pi(k_\mathrm{F}R_\mathrm{eff})^2} - 1]^{-1/2}, \quad (20)$$

showing that the scattering length increases as $R_\mathrm{eff}^2$ is reduced while keeping the chemical potential fixed. We will use these results to compare the mean-field prediction with our diffusion Monte Carlo estimate for the ground-state energy at the BEC-BCS crossover as a function of the effective range in Sec. IV.

## III. PSEUDOPOTENTIALS

To address the full gamut of effective ranges, we turn to numerical quantum Monte Carlo simulations. For our quantum Monte Carlo simulation of the strongly interacting regime, we eliminate the need to simulate the bosonic particles by using a single-channel Hamiltonian that only includes the spin-1/2 fermions,

$$\hat{H}^{1-\mathrm{ch}} = -\frac{1}{2}\sum_{i=1}^{N}\nabla_i^2 + \sum_{i<j}^{N} V(r_{ij}). \quad (21)$$

$\nabla_i^2$ is the Laplacian with respect to the coordinates of particle $i$, $N$ is the total number of particles, and we study equal numbers of up and down spin particles. $r_{ij}$ is the distance between particles $i$ and $j$, and $V$ is an attractive interaction potential that acts between particles with opposite spins. The aim of this section is to develop a real-space form $V(\mathbf{r})$ that scatters a pair of fermions with the desired $s$-wave scattering phase shift characterized by the scattering length $a$ and effective range $R_\mathrm{eff}$.

The scattering phase shift for scattering length $a = 1$ and effective range squared $R_\mathrm{eff}^2 = \{-1,0,1\}$ is plotted in Fig. 1 (all length scales are in units of inverse momentum). The cases for $R_\mathrm{eff}^2 = 0$ and $R_\mathrm{eff}^2 = 1$ are qualitatively similar, while the case for $R_\mathrm{eff}^2 = -1$ differs by the absence of the phase winding by $\pi$. Furthermore, as $|R_\mathrm{eff}^2|$ becomes larger, the phase shift

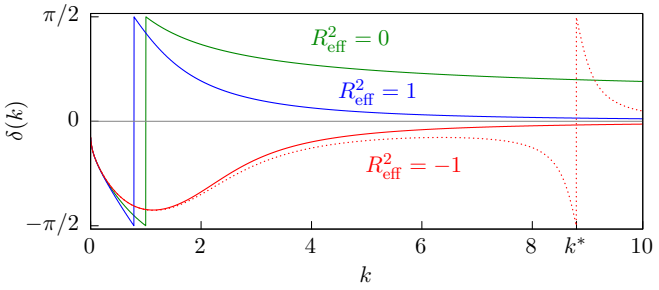


FIG. 1. Scattering phase shift $\delta(k)$ for $a=1$ and $R^2_{\rm eff}=\{-1,0,1\}$ (all lengths are in units of inverse momentum). For $R^2_{\rm eff}=-1$ the phase shift of a realistic potential with the same low-energy scattering properties is indicated by the red dotted line. The noninteracting phase shift is shown by the gray dashed line.

decays more rapidly towards zero for large $k$, as expected for the noninteracting limit $|R^2_{\rm eff}|\to\infty$.

The absence of the phase winding of $\pi$ for the case $R^2_{\rm eff}=-1$ has an important consequence because the number of phase windings is related to the number of bound sates $n$ by Levinson's theorem [36],

$$\delta(0)-\delta(\infty)=n\pi. \tag{22}$$

Attractive interactions in two dimensions [37] exhibit at least a single bound state [38,39], so $n\geqslant 1$. The scattering phase shift of the desired attractive interaction therefore should include at least a single phase winding, but as it stands this is not the case for $R^2_{\rm eff}=-1$ because $\delta(0)-\delta(\infty)=0$. A physical potential must, however, have a phase winding at $k^*$ as indicated by the dashed line in the figure, which corresponds to adding a higher-order term to the expansion of $\cot(\delta(k))$. Similar to the 3D case reported in Ref. [30], this additional phase winding does not affect the phase shift at low momenta, and provided $k^*$ is much larger than any other momentum scale in the system, i.e., the Fermi momentum $k_{\rm F}$ for a fermionic many-body system, does not alter the physics of the system as the interacting particles cannot probe these high momentum features. For $R^2_{\rm eff}>(4a^2)/(\pi {\rm e})$, Levinson's theorem has another important consequence as the bound-state energy, Eq. (12), does not exist because $W_0$ does not exist for $z<-1/{\rm e}$. The absence of the bound state violates Levinson's theorem, which implies that no real-space potential exists in this regime.

To describe interactions with effective range $-1.5\leqslant k_{\rm F}^2R^2_{\rm eff}\leqslant 0$, we develop a pseudopotential that is smooth and extended in space to aid the numerical convergence, and accurately reproduces the scattering phase shift and bound-state energy. We first discuss the potential well as it is commonly used to simulate Fermi gases with contact interactions, before introducing the UTP [28–30,40,41] as a model potential for both zero and finite effective interaction range. Because of its high accuracy, wide spatial extent, and smoothness, we select the UTP for our numerical study.

### A. Potential well

A potential well was used in Refs. [21,42,43] to model the contact interaction obtained in the zero effective-range limit $R^2_{\rm eff}=0$,

$$V(r)=\begin{cases}-U, & r\leqslant r_{\rm c},\\ 0, & r>r_{\rm c},\end{cases} \tag{23}$$

with depth $U$ and radius $r_{\rm c}$. The depth $U$ can be tuned to give the correct scattering length $a$, while the effective range $R^2_{\rm eff}$ is proportional to $r_{\rm c}^2$ and thus positive [33]. To ensure that the effective range term is small, Bertaina and Giorgini [21] used $k_{\rm F}r_{\rm c}=2.5\times10^{-3}$. The discontinuity of the potential well at $r_{\rm c}$ can be avoided by using a smooth form $V(r)=a/\cosh^2(br)$ with $a<0$ [23,44], but this does not change the essence of the problem as the potential remains uniformly attractive and must be deep and narrow to ensure small $R^2_{\rm eff}$. With a small effective radius both potentials are difficult to handle numerically so we propose the UTP as an alternative that allows $R^2_{\rm eff}$ to be varied independently of $r_{\rm c}^2$.

### B. UTP

We now propose a pseudopotential that gives the precise scattering phase shift and bound-state energy for $-1.5\leqslant k_{\rm F}^2R^2_{\rm eff}\leqslant 0$. Furthermore, the potential is smooth and extended in space, easing the application of numerical methods. Following Refs. [28–30], we propose a UTP that takes a polynomial form within a cutoff radius $r_{\rm c}$,

$$V^{\rm UTP}(r)=\begin{cases}\left(1-\frac{r}{r_{\rm c}}\right)^2\left[u_1\left(1+\frac{2r}{r_{\rm c}}\right)+\sum_{i=2}^{N_{\rm u}}u_i\left(\frac{r}{r_{\rm c}}\right)^i\right], & r\leqslant r_{\rm c},\\ 0, & r>r_{\rm c},\end{cases} \tag{24}$$

where the $u_i$ are the $N_{\rm u}=3$ optimizable coefficients. The term $(1-r/r_{\rm c})^2$ ensures that the UTP goes smoothly to zero at $r=r_{\rm c}$, and the component $u_1(1+2r/r_{\rm c})$ constrains the pseudopotential to have zero gradient at particle coalescence to ensure that the wave function is smooth.

The coefficients $\{u_i\}$ are optimized by solving the Schrödinger equation for the two-body problem numerically [29,30]. We minimize a cost function $F$ containing two terms: (i) The difference of the logarithmic derivative of the pseudopotential wave function with the exact wave function evaluated at the exact bound-state energy $E_{\rm b}$ and the cutoff radius $r_{\rm c}$. This term serves to obtain the correct bound state-wave function, and therefore binding energy. (ii) The difference in scattering phase shift between the pseudopotential and the exact expression, summed over angular momentum channels $l$ and averaged over the Fermi sea $0\leqslant k\leqslant k_{\rm F}$ weighted by the density of scattering states in the center of mass frame $g(x)=8x\{1-\frac{2}{\pi}[x\sqrt{1-x^2}+\arcsin(x)]\}$ [29],

$$F=r_{\rm c}^2\left|\frac{d[\ln(\psi^{\rm UTP})]}{dr}-\frac{d[\ln(\psi)]}{dr}\right|^2_{E=E_{\rm b},r=r_{\rm c}}+\frac{1}{\pi}\sum_l\int_0^{k_{\rm F}}\left|\delta_l^{\rm UTP}(k)-\delta_l(k)\right|^2g(k/k_{\rm F})dk. \tag{25}$$

The prefactors $r_{\rm c}^2$ and $1/\pi$ serve to make both terms dimensionless. The upper momentum cutoff for the integral determines up to which momentum scale the UTP will accurately reflect the desired phase shift and its value influences features of the

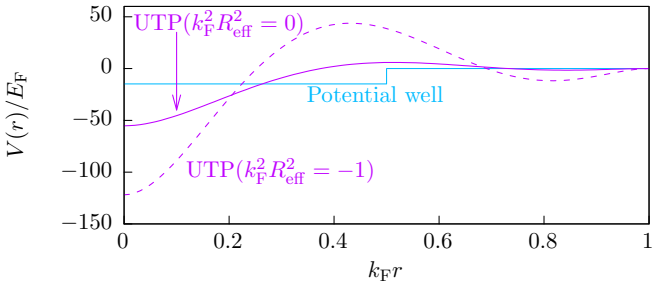


FIG. 2. Plot of the potential well (blue), the UTP for the contact interaction $(k_F R_{eff})^2 = 0$ (solid purple), and the UTP for finite effective range $(k_F R_{eff})^2 = -1$ (dashed purple), normalized by the reciprocal Fermi energy $E_F$ as a function of the dimensionless radius. All potentials are calibrated for interaction strength $\ln(k_F a) = 0$.

phase shift at high momenta including the value of $k^*$. We have confirmed that our results are insensitive to the value of the cutoff and $k^*$.

While increasing the cutoff radius $r_c$ improves numerical performance, it also introduces higher systematic error. In particular, the cutoff radius should be chosen less than the interparticle spacing so that three-body scattering events are rare; we therefore follow the approach by Refs. [28–30] and set $r_c = 1/k_F$ to balance statistical and systematic errors in the QMC results.

### C. Comparison of potentials

We compare the real-space forms of the potential well and UTP in Fig. 2 with $\ln(k_F a) = 0$. We have chosen the cutoff radius of the potential well $r_c = 1/(2k_F)$, such that its spatial extent is similar to that of the UTP and so the computational efficiency should be comparable. The potential well was used in previous works [21] to represent the contact interaction, although it has $R_{eff}^2 > 0$. The UTP is shown for both the zero range limit $k_F^2 R_{eff}^2 = 0$ and for negative effective range squared $k_F^2 R_{eff}^2 = -1$. Comparing the potential well with the UTP for $k_F^2 R_{eff}^2 = 0$, the potential well is shallower than the UTP at small radius, but deeper at intermediate radius and furthermore displays a discontinuity at the cutoff radius. In contrast, the UTP is smooth throughout, easing the numerical optimization process of the variational wave function. Reducing $k_F^2 R_{eff}^2$ from 0 to $-1$, the UTP develops a potential barrier at intermediate radius. The barrier suppresses quantum tunneling between the composite two-fermion bound state at small radius and the continuum of scattering states at large radius. This physics was seen in the two channel model as $\lambda \to 0$, and furthermore is reminiscent of the physics for negative effective range in three dimensions [30].

We next compare the accuracy of the bound-state energy and scattering phase shift of the pseudopotentials, shown in Fig. 3. The error in the bound-state energy for the UTP is less than $10^{-6}$ in the zero effective-range limit and less then $10^{-4}$ for $k_F^2 R_{eff}^2 = -1$ for all interaction parameters $\ln(k_F a)$. Moreover, the error in the bound-state energy decreases when reducing the interaction parameter $\ln(k_F a)$ below zero. This regime corresponds to a BEC state of tightly bound bosons for the many-body system, and we therefore expect the

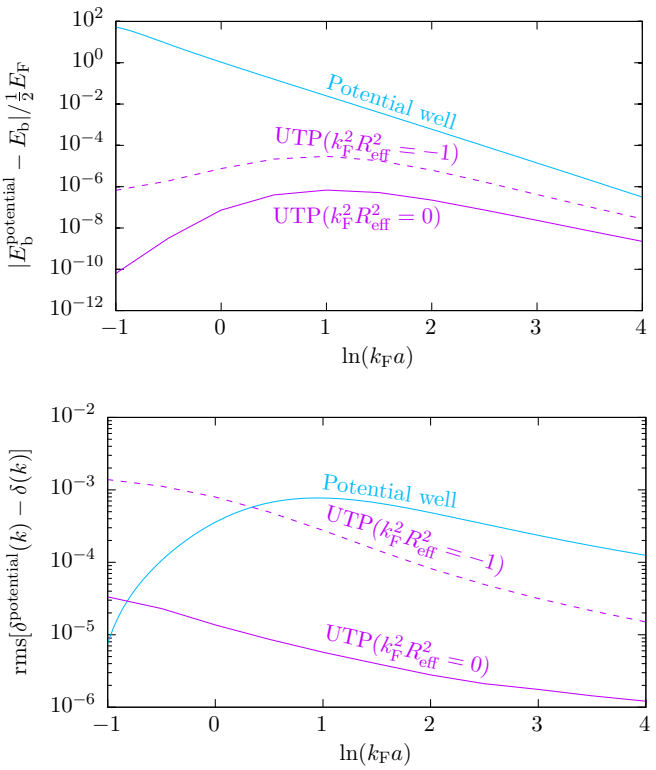


FIG. 3. (Top) Difference in absolute value of the bound-state energy of the potential and the exact bound-state energy of the potential well (blue), the UTP for the contact interaction $(k_F R_{eff})^2 = 0$ (solid purple), and the UTP for finite effective range $(k_F R_{eff})^2 = -1$ (dashed purple). (Bottom) Root-mean-square (rms) scattering phase-shift error of the same potentials, with $k$ averaged over the interval from zero to the Fermi momentum $k_F$.

potentials to accurately describe this region. In contrast, the bound-state energy error for the potential well is much larger, and increases when approaching the BEC regime. Turning to the root-mean-square (rms) scattering phase-shift error, accuracy is most important for the BCS regime $\ln(k_F a) > 0$ of weakly bound particles, where scattering is abundant. In this regime, we observe that the rms error is two orders of magnitude smaller for the UTP in the zero effective-range limit compared with the potential well, despite the fact that the potential well is calibrated to yield the correct scattering length. The error of the UTP for $k_F^2 R_{eff}^2 = -1$ is about two orders of magnitude larger at $\ln(k_F a) = -1$ compared to the UTP for $k_F^2 R_{eff}^2 = 0$, but decreases to only one order of magnitude at $\ln(k_F a) = 4$ as we move towards the BCS regime.

We conclude that the UTP in the zero-range limit has a smaller error in the bound-state energy and average scattering phase shift than an analogous potential well. Furthermore, the UTP evolves smoothly as a function of the effective range, while the potential well cannot deliver negative $k_F^2 R_{eff}^2$. We therefore select the UTP for our numerical study.

## IV. QUANTUM MONTE CARLO

To calculate the ground-state properties of the Fermi gas in the strongly interacting regime we use the CASINO implementation of the fixed-node diffusion Monte Carlo (DMC)

algorithm [45]. DMC is a Green's function projector method that produces a variational upper bound on the ground-state energy, depending only on the nodes of the trial wave function [46–48]. We start from the Slater-Jastrow trial wave function $\Psi = \mathrm{e}^J D$ introduced in Ref. [30]. $D$ is a Slater determinant of $N/2$ pairing orbitals $\phi(\mathbf{r}_{ij})$, each holding an up- and down-spin particle and $\mathbf{r}_{ij}$ the separation between them, and $\mathrm{e}^J$ a Jastrow factor that captures correlations between particles. The pairing orbitals are formed of a linear combination of plane waves, compatible with the nearly free electron gas in the BCS limit, and a polynomial term, suitable for describing the weakly interacting composite bosons in the BEC regime. We use a back-flow transformation to capture many-body correlations in the pairing orbitals [49]. The trial wave function includes a total of 33–39 parameters depending on the number of particles simulated, which we optimize first using variational Monte Carlo (VMC) before using it as input for our DMC calculations.

We calculate the ground-state wave function for systems with 26 and 58 particles as in Refs. [21,23], and also for a system of 98 particles to allow us to accurately extrapolate to the thermodynamic limit. We also extrapolate to zero time-step and infinite walker populations; details are provided in Appendix B. We expect that the use of a quadratic DMC algorithm would give similar results [50,51]. Expectation values of operators that do not commute with the Hamiltonian are computed using the extrapolated estimator $\langle \hat{A} \rangle = 2\langle \hat{A} \rangle_{\mathrm{DMC}} - \langle \hat{A} \rangle_{\mathrm{VMC}}$, such that the residual bias is quadratic in the difference between the VMC and DMC wave functions for the part of the operator that is local in position space [52–54]. The extrapolated estimates are within the statistical error bars of the bare DMC estimates unless indicated otherwise, and we expect residual errors to be small.

In the limit $k_{\mathrm{F}}^2 R_{\mathrm{eff}}^2 = 0$ the Slater-Jastrow trial wave function captures at least 92% of the correlation energy, defined as the difference between the Hartree-Fock and DMC ground-state energy, which is raised to 96% using back-flow transformations. For finite effective ranges back-flow transformations are especially important, as the amount of correlation energy captured at the BEC-BCS crossover point without back flow reduces from 95% to 91% while decreasing $k_{\mathrm{F}}^2 R_{\mathrm{eff}}^2$ from 0 to $-1.5$, but remains at a constant 97% using back-flow transformations.

### A. Zero-range limit

To demonstrate the accuracy of the proposed pseudopotential in combination with our trial wave function, we first explore the ground-state energy of the gas across the BEC-BCS crossover in the zero effective-range limit. This limit has been studied before using DMC methods by Refs. [21,23] and also using the auxiliary-field quantum Monte Carlo (QMC) method that is free from the sign problem for spin-balanced systems with attractive interactions by Ref. [22]. The BEC-BCS crossover is parameterized in two dimensions by the interaction parameter $\ln(k_{\mathrm{F}}a)$, which is inversely proportional to the mean-field interaction strength [25,26]. We study the ground-state energy per particle $E$ minus half the two-body binding energy $E_{\mathrm{b}}$, normalized by the energy per particle of a noninteracting gas $E_{\mathrm{F}}/2$. Figure 4 shows that the relative energy increases smoothly as the interaction parameter $\ln(k_{\mathrm{F}}a)$ is increased from negative values on the BEC side to positive values on the BCS side. The polynomial fits to the data points are obtained by explicitly taking into account the asymptotic functional forms in the BEC and BCS limits as detailed in Refs. [22,23].

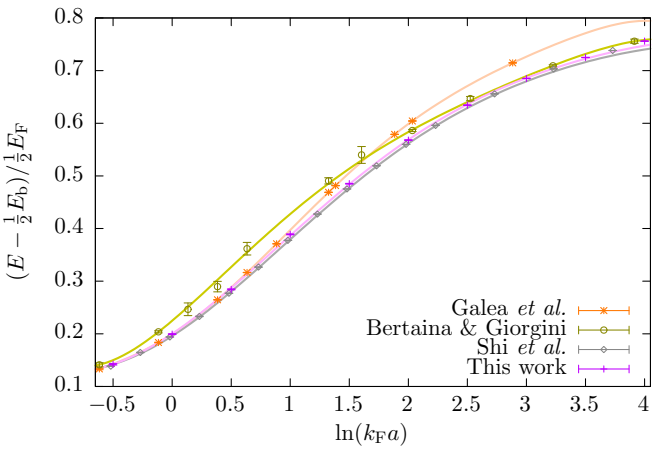


FIG. 4. Ground-state energy per particle minus half the two-body binding energy, divided by the energy per particle in a noninteracting gas, as a function of the interaction parameter $\ln(k_{\mathrm{F}}a)$ across the BEC-BCS crossover. Next to our result we show the results from Refs. [21–23].

By virtue of our pairing orbital that can smoothly interpolate between the BCS and BEC limits we obtain a trial wave function that provides the lowest DMC upper bound on the ground-state energy to date. We benefit from our smooth pseudopotential in the regime $0 \lesssim \ln(k_{\mathrm{F}}a) \lesssim 2$ where interactions are strong, while for $2 \lesssim \ln(k_{\mathrm{F}}a)$ we find that the finite-size correction leads to a significant reduction of the ground-state energy, and our results are therefore lower than those reported by Galea *et al.* [23] (see Appendix B 2 for details). The reported DMC energies are close to the auxiliary-field QMC results from Shi *et al.* [22], indicating that the fixed-node error is small.

An important ramification of the contact interaction in the zero-range limit is the universal constant called the contact $C$, which for example describes the high-momentum tail of the momentum distribution, $n(k) \sim C/k^4$ [55]. It is proportional to the derivative of the equation of state,

$$\frac{C - C_0}{k_{\mathrm{F}}^4} = \frac{1}{2}\frac{d[E/E_{\mathrm{F}}]}{d[\ln(k_{\mathrm{F}}a)]} - \frac{1}{2}\frac{d[(E_{\mathrm{b}}/2)/E_{\mathrm{F}}]}{d[\ln(k_{\mathrm{F}}a)]}. \tag{26}$$

Here $C_0$ is the contribution to the contact from the composite boson that occurs at the mean-field level [21]. The contact is shown in Fig. 5 and attains a maximum value at $\ln(k_{\mathrm{F}}a) \approx 0.8$. As a result of our lower upper bound on the ground-state energy, our reported maximum value of the contact is lower than earlier DMC studies [21,23] and agrees well with the auxiliary-field QMC result from Shi *et al.* [22].

#### *1. Condensate fraction*

A defining feature of a superconductor is the existence of a condensate that correlates pairs of fermions with opposite

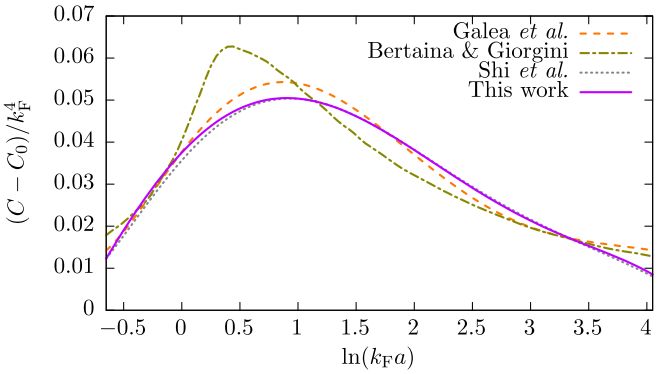


FIG. 5. Contact minus the contact contribution from the molecular bound state, normalized by the fourth power of the Fermi wave vector. For comparison we also show the results from Refs. [21–23].

spins irrespective of the distance between them. Correlations between particles are naturally captured in the two-body density matrix,

$$\rho^{(2)}_{\alpha\beta}(\mathbf{r}'_1,\mathbf{r}'_2;\mathbf{r}_1,\mathbf{r}_2) = \langle c^\dagger_\alpha(\mathbf{r}'_1)c^\dagger_\beta(\mathbf{r}'_2)c_\beta(\mathbf{r}_2)c_\alpha(\mathbf{r}_1)\rangle, \qquad (27)$$

where $c^\dagger_\alpha(\mathbf{r})$ is the fermionic creation and $c_\alpha(\mathbf{r})$ the annihilation operator for a particle with spin $\alpha$ at position $\mathbf{r}$. The condensate fraction is defined as $c = 2n_0/n$, where the condensate density $n_0$ is the largest eigenvalue of the two-body density matrix for particles with opposite spins and $n$ is the density [58], which we compute using the improved estimator of Ref. [30].

We show the extrapolated estimate together with the bare VMC and DMC estimates in Fig. 6. For comparison we also plot the Bogoliubov perturbation theory for the BEC limit [56] and the mean-field prediction [57]. Furthermore, we show the auxiliary-field QMC results of Shi *et al.* [22]. Starting from the BCS regime where $\ln(k_F a)$ is large so interactions are weak, the condensate fraction increases exponentially as $\ln(k_F a)$ is reduced. Our result is higher than the mean-field prediction for $\ln(k_F a) \gtrsim 2.4$, while for $\ln(k_F a) \lesssim 2.4$ the computed condensate fraction is lower than the mean-field result and approaches the Bogoliubov result near $\ln(k_F a) = -0.5$. The

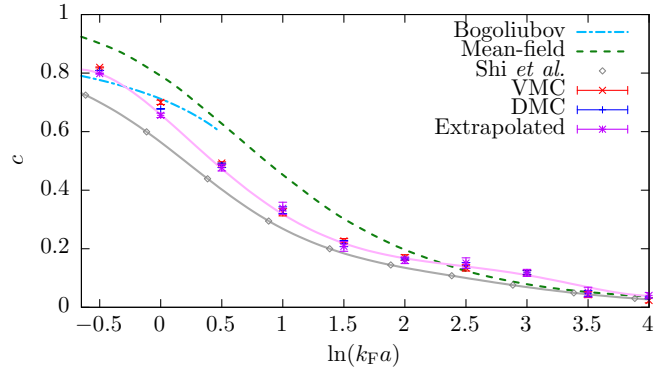


FIG. 6. Condensate fraction as a function of the interaction parameter $\ln(k_F a)$. We show the VMC, DMC and extrapolated estimates, along with the auxiliary-field quantum Monte Carlo result from Shi *et al.* [22]. Also shown are the perturbative Bogoliubov theory for the BEC limit [56] and the mean-field prediction [57].

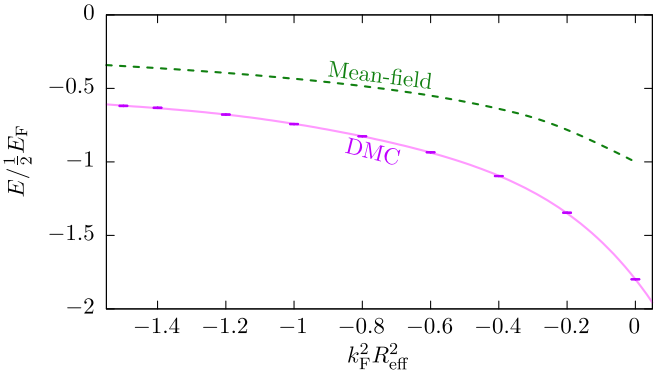


FIG. 7. DMC ground-state energy per particle in units of that of a noninteracting gas as a function of the dimensionless effective range squared $k_F^2 R_{eff}^2$ shown by the solid purple line. The mean-field result is shown by the dashed green line.

results computed using the extrapolated estimator are similar to the bare VMC and DMC results, except near the BEC-BCS crossover point $\ln(k_F a) = 0$ where the correction is significant. Our results are higher than those reported by Shi *et al.* [22], although both results converge to the mean-field theory as $\ln(k_F a) \to 4$. The disagreement could be the result of the fixed-node approximation employed in this paper, or the lattice structure and corresponding breaking of rotational symmetry introduced by Shi *et al.* [22].

### B. Finite effective range

Having demonstrated how the accurate scattering properties, smoothness, and spatial extent of our pseudopotential result in precise quantum Monte Carlo results in the familiar zero effective-range limit, we now exploit the UTP to analyze interactions with a finite effective range. We study the ground-state wave function as a function of the effective range along the BEC-BCS crossover by adjusting $a$ to follow the trajectory defined by $\mu = 0$ in mean-field approximation. We expect the actual trajectory of $\mu = 0$ when calculated beyond mean-field approximation to track different values of $a$, as has been found for $k_F^2 R_{eff}^2 = 0$ [21,23]. At finite effective range, we expect a similar shift, which approaches zero as $k_F^2 R_{eff}^2 \to -\infty$, where the mean-field theory becomes exact.

The DMC ground-state energy is shown as a function of the effective interaction-range squared $k_F^2 R_{eff}^2$ in Fig. 7 together with the mean-field prediction. Starting at the point $k_F^2 R_{eff}^2 = 0$ considered before, we observe that the DMC estimate considerably improves the mean-field estimate $E = -E_F/2$ by including additional correlations between particles, reducing the energy to $E = -1.797(1)E_F/2$. As the effective range becomes more negative, correlations beyond the mean-field level diminish and the DMC result approaches the mean-field result. The energy increases towards zero in the limit $k_F^2 R_{eff}^2 \to -\infty$ where the ground state is a condensate of noninteracting composite bosons, each with zero internal binding energy.

#### 1. *Condensate fraction*

The VMC, DMC, and extrapolated estimates for the condensate fraction are shown as a function of $k_F^2 R_{eff}^2$ in Fig. 8.

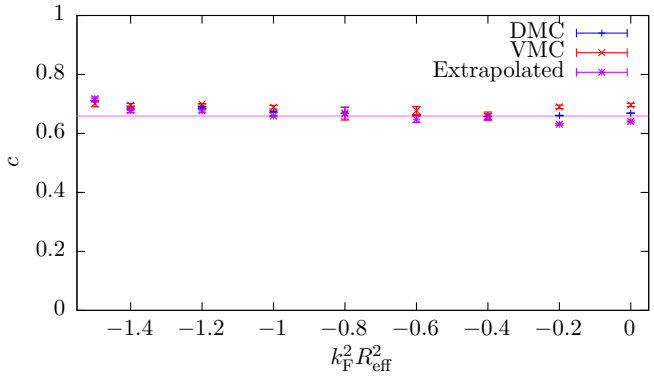


FIG. 8. Condensate fraction as a function of the dimensionless effective range squared. We show the extrapolated result, as well as the bare VMC and DMC estimates.

The extrapolated estimator agrees with the VMC and DMC results, except near the zero effective-range limit considered before. We observe that at the BEC-BCS crossover point in mean-field approximation the condensate fraction remains constant at $c \approx 0.7$ for values of the effective range squared $-1.5 \leqslant k_F^2 R_{eff}^2 \leqslant 0$. This is consistent with our choice to tune $a$ and $R_{eff}$ to run along the BEC-BCS cross-over line, and is also observed in a three-dimensional system where a vanishing slope is seen at small negative effective range [30]. For large negative values of $k_F^2 R_{eff}^2$, we expect the condensate fraction to decline as the mean-field theory predicts $c \to 0$ in the limit $k_F^2 R_{eff}^2 \to -\infty$ where the theory becomes noninteracting and correlations vanish.

### 2. *Momentum distribution*

Figure 9 shows the results of the extrapolated estimator for the momentum distribution $n(k)$ for $k_F^2 R_{eff}^2 \in \{0, -1\}$ with an inset plot that shows DMC, VMC, and extrapolated data separately for $k_F^2 R_{eff}^2 = 0$ (top), and the tail of the distributions for $k > 3.0 k_F$ on logarithmic axes (bottom).

Both momentum distributions are different from a noninteracting Fermi distribution, similar to what was found by Shi *et al.* [22] for $k_F^2 R_{eff}^2 = 0$. The distribution has a widespread tail for large momenta, and it is significantly reduced for momenta less than $k_F$, which illustrates the formation of composite bosons. We expect the high momentum components induced by the composite bosons to be accurately described by our UTP as it delivers the correct two-body binding energy.

The extrapolation leads to small corrections only, with the most significant corrections occurring near zero and the Fermi momentum. This reflects the high quality of our trial wave function and we expect residual errors to be small.

For $k_F^2 R_{eff}^2 = 0$, a curve of $n(k) = C/k^4$ is shown in the logarithmic plot, where the value of $C/k_F^4 = 1.03$ has been extracted from the results that we obtained from Eq. (26). The plotted line agrees well with the QMC data within error bars and this is expected for $k_F^2 R_{eff}^2 = 0$. For $k_F^2 R_{eff}^2 = -1$, the tail of the momentum distribution decays less rapidly before the $n \sim k^{-4}$ regime is entered at $k/k_F \approx 7$. A least-squares fit of $n(k) = C/k^4$ taking into account data for $k/k_F > 7$ determines $C/k_F^4 = 4.64(4)$, and agrees well with the data within error bars. The rise of the contact is expected as $k_F^2 R_{eff}^2$ is reduced

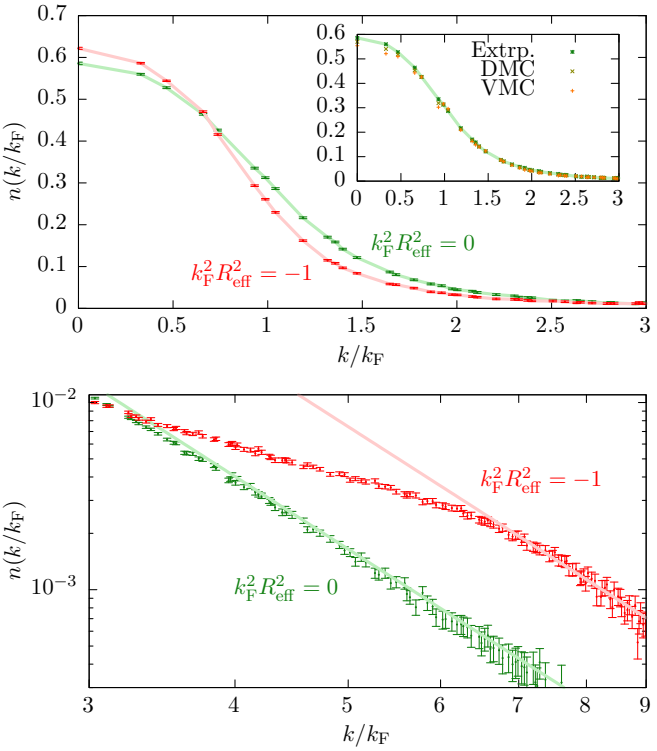


FIG. 9. (Top) Extrapolated data for the momentum distribution $n(k)$ for $k_F^2 R_{eff}^2 \in \{0, -1\}$. The inset additionally shows DMC, VMC, and extrapolated results separately for $k_F^2 R_{eff}^2 = 0$. (Bottom) Tail of the momentum distribution on logarithmic axes, with the lines indicating $n(k) \sim 1/k^4$.

due to the conversion of fermions to bosons, akin to the 3D case [30]. The $n(k) \sim k^{-4}$ dependency for arbitrary effective range was demonstrated by Refs. [30,59] in three dimensions, and the QMC results studied here suggest that this extends to two dimensions. In both cases, we expect the $n(k) \sim k^{-4}$ dependency to hold only up to a certain momentum scale, and in particular not beyond the momentum scale up to which the UTP was optimized.

### 3. *Pair-correlation function*

The pair-correlation function (PCF) for two fermions is obtained from the two-body density matrix as $g_{\alpha\beta}(\mathbf{r}) = \rho^{(2)}_{\alpha\beta}(\mathbf{r}' + \mathbf{r}, \mathbf{r}'; \mathbf{r}' + \mathbf{r}, \mathbf{r}')/(n/2)^2$. Figure 10 shows the results of the extrapolated estimator for the PCF for opposite (top) and equal (bottom) spins for $k_F^2 R_{eff}^2 \in \{-1, 0\}$ together with the result for noninteracting fermions. The insets show DMC, VMC, and extrapolated data separately for $k_F^2 R_{eff}^2 = 0$.

For opposite spins, we correct the PCF for short-range effects due to the particular form of the UTP [30,40]

$$g_{\uparrow\downarrow}(r) = \frac{g^{2-\text{body,exact}}_{\uparrow\downarrow}(r)}{g^{2-\text{body,UTP}}_{\uparrow\downarrow}(r)} g^{\text{QMC}}_{\uparrow\downarrow}(r), \tag{28}$$

where $g^{2-\text{body,}\{\text{exact,UTP}\}}_{\uparrow\downarrow}(r)$ are the PCF for the two-body problem computed using the exact and UTP wave functions, respectively, and $g^{\text{QMC}}_{\uparrow\downarrow}(r)$ is the uncorrected QMC result for the PCF. Since our UTP is norm-conserving [28–30],

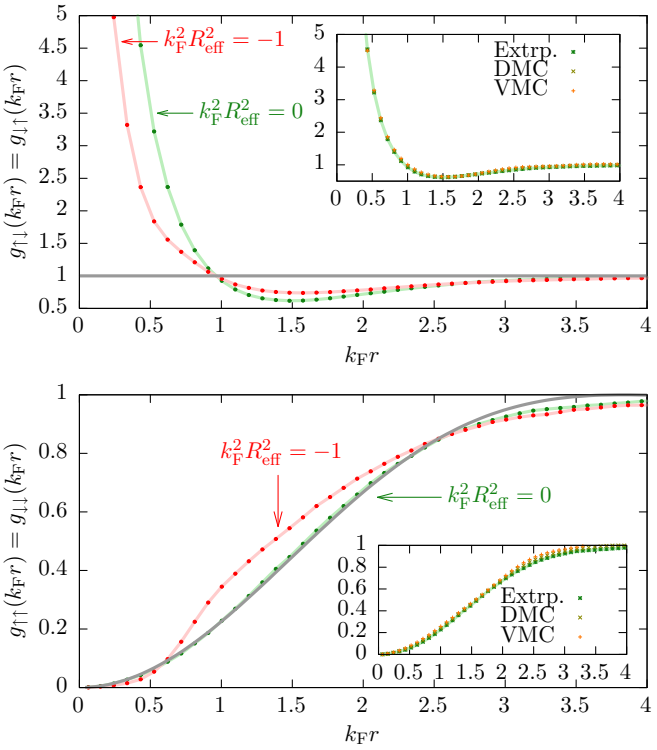


FIG. 10. Pair-correlation function for opposite (top) and equal (bottom) spins for $k_F^2 R_{eff}^2 \in \{-1,0\}$. The noninteracting correlation function for fermions is indicated by the gray dashed line. The insets show DMC, VMC, and extrapolated data separately.

no correction is necessary outside of the interaction region. Similar to the momentum distribution, the extrapolation from DMC and VMC data results in minor corrections only.

The PCF for opposite-spin species shows a significant increase at short distances ($k_F r < 1$). This is due to the attractive potential, and indicates the formation of composite bosons. The PCF is reduced accordingly for intermediate distances ($k_F r \approx 1.5$). When $R_{eff}^2$ becomes more negative, the fermions become more tightly bound into bosons, but the residual interactions between two composite bosons diminishes. As the conversion of fermions into noninteracting pointlike bosons progresses, the correlations between two fermions are limited to a decreasing distance as is illustrated in the figure for $k_F^2 R_{eff}^2 = -1$.

For equal spins, the result for $k_F^2 R_{eff}^2 = 0$ is similar to the noninteracting case, which comprises the exchange-correlation hole due to Pauli exclusion. When decreasing the effective range to $k_F^2 R_{eff}^2 = -1$, the fermions are more tightly bound as composite bosons and the PCF is increased at short distances, reducing the distortion caused by the exchange-correlation hole and approaching the PCF of noninteracting bosons.

## V. DISCUSSION

We investigated the many-body ground state of a two-dimensional Fermi gas across the BEC-BCS crossover as a function of the effective interaction range. A mean-field theory was developed showing that in the limit $k_F R_{eff}^2 \to -\infty$ the fermions gain energy by pairing into composite bosons in order to escape from the Fermi sea. This should be contrasted with the noninteracting BEC found in the limit $\ln(k_F a) \to -\infty$, where the binding energy of the fermions diverges. Quantitatively accurate results are obtained for the superconducting energy gap, chemical potential, and ground-state energy using the mean-field theory for $k_F^2 R_{eff}^2 \ll -1$.

To study the strongly interacting regime $-1.5 \leqslant k_F^2 R_{eff}^2 \leqslant 0$ using DMC, we proposed the ultratransferable pseudopotential that produces the correct scattering phase shift and bound-state energy. We first revisited the case $k_F^2 R_{eff}^2 = 0$, where we obtained the lowest DMC variational estimate of the ground-state energy and confirmed that the fixed-node error is small. We showed that the ground-state energy approaches the mean-field prediction when the effective range is reduced, and showed signatures for the formation of composite bosons in the momentum distribution and pair-correlation functions. We confirmed the tail of the momentum distribution $\sim 1/k^4$ for $k_F^2 R_{eff}^2 = 0$ and demonstrated the same asymptotic form holds for $k_F^2 R_{eff}^2 < 0$, as was previously observed in three dimensions [30,59].

While the mean-field theory provides qualitative insights into finite interaction range effects and is also quantitatively trustworthy for $k_F^2 R_{eff}^2 \ll -1$, we expect that our proposed ultratransferable pseudopotential will be useful for future quantitative studies of the strongly interacting regime for smaller negative values of $k_F^2 R_{eff}^2$. The results presented for zero and finite effective ranges should be relevant to ultracold-atom experiments using broad and narrow Feshbach resonances, respectively.

## ACKNOWLEDGMENTS

The authors thank T. Whitehead, R. Needs, S. Giorgini, J. Boronat, and N. Drummond for useful discussions. The authors acknowledge the financial support of the Engineering and Physical Sciences Research Council (EPSRC) Grant No. [EP/J017639/1], L.M.S. acknowledges financial support from the Cambridge European Trust, Cambridge Philosophical Society, VSB Fonds, and the Prins Bernhard Cultuurfonds, and G.J.C. acknowledges the financial support of the Royal Society and Gonville & Caius College. Computational facilities were provided by the University of Cambridge High Performance Computing Service. The software to generate the UTP and the data used in this work are available online [60].

## APPENDIX A: BEC AND BCS LIMITS AT FINITE INTERACTION RANGE

In this section, we consider the limits of a small energy gap $\Delta$ corresponding to the BEC (negative chemical potential) and BCS (positive chemical potential) regimes.

*1. BEC limit.* The chemical potential approaches $E_b/2$ and is therefore negative, so $\mathrm{sgn}(\mu/\Delta) = -1$, while its magnitude is large, so $|\mu/\Delta| \gg 1$. Expanding around $\mu/\Delta = -\infty$, the gap and number equations read

$$B = \frac{2|\mu|}{\lambda}\sqrt{-\frac{4\pi}{\lambda^2}(\omega_0 - 2\mu) + \ln\left(\frac{k_F^2}{2|\mu|}\right)}, \quad \text{(A1a)}$$

$$n = \left(2 + \frac{\lambda^2}{4|\mu|}\right)B^2. \quad \text{(A1b)}$$

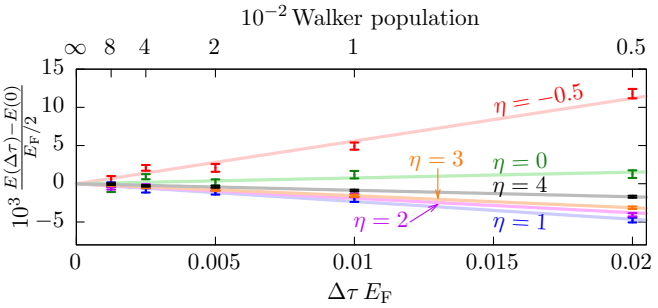


FIG. 11. Variation of the dimensionless ground-state energy per particle with DMC time step and walker population with interaction parameter $\eta = \ln(k_F a)$ in the zero-range limit $k_F^2 R_{\rm eff}^2 = 0$. The straight lines show a weighted least-squares fit to the data points.

*2. BCS limit.* In the BCS limit the chemical potential approximately equals the Fermi energy $\mu \simeq E_F$, so $\mathrm{sgn}(\mu/\Delta) = 1$ while the gap is exponentially weak so $|\mu/\Delta| \gg 1$. Expanding the gap and number equations we find

$$B = \sqrt{2k_F^2\mu}\exp\left[-\frac{2\pi}{\lambda^2}(\omega_o - 2\mu)\right], \tag{A2a}$$

$$n = 2B^2 + \frac{\mu}{\pi}. \tag{A2b}$$

Since $B$ is exponentially small, the number equation confirms that the chemical potential approximately equals the Fermi energy as $n = k_F^2/(2\pi)$.

## APPENDIX B: DMC EXTRAPOLATIONS

To accurately extract the ground-state energy, it is important to extrapolate to zero time step and infinite walker population, and to the thermodynamic limit.

### 1. Time step and walker population extrapolation

We simultaneously extrapolate to zero time step and infinite walker population to eliminate the bias of the DMC algorithm, resulting from the application of the imaginary time evolution operator $e^{-\hat{H}\Delta\tau}$ at finite time steps $\Delta\tau$ on a trial wave function represented by a finite number of walkers [48,61]. The absolute value of the gradient of the energy with respect to time step is expected to be proportional to the local energy variance, which measures the error made in using the trial wave function to describe the true ground state [40,41]. We simultaneously reduce the time step by a factor of 2 and increase the walker population by the same factor, as seen in Fig. 11, where we demonstrate our procedure for several values of the interaction parameter $\eta = \ln(k_F a)$ for $k_F^2 R_{\rm eff}^2 = 0$. As expected, the variation with time step is smallest for $\eta = 4$, where the trial wave function accurately captures the weakly interacting ground state of the system, and gradually increases as $\eta$ is decreased. The gradient changes sign near $\eta = 0$ before attaining its maximum magnitude for the interactions parameters studied at $\eta = -0.5$. The error introduced in the dimensionless ground-state energy by using a finite time step and walker population increases from $0.5\times10^{-1}\Delta\tau\, E_F$ for $\eta = 4$ to $2.5\times10^{-1}\Delta\tau\, E_F$ for $\eta = -0.5$. Extrapolation is therefore essential for time steps $\Delta\tau\, E_F > 4\times10^{-3}$ where this exceeds the uncertainty in the extrapolation $< 10^{-3}$.

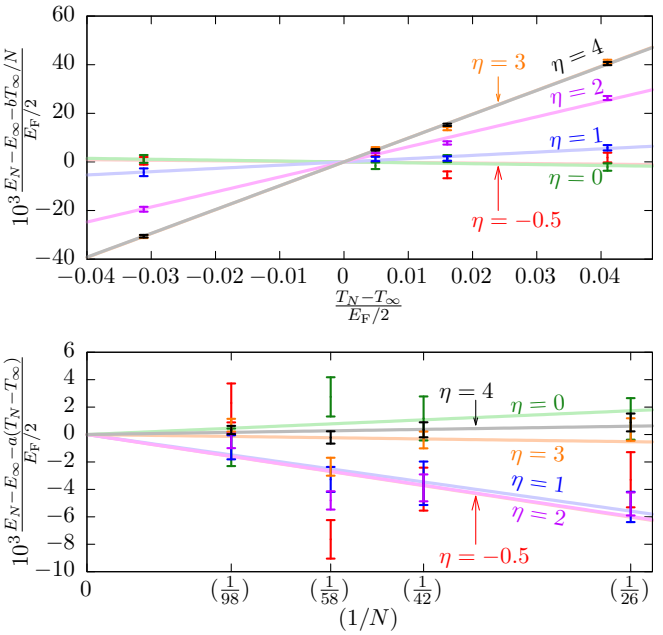


FIG. 12. Variation of the dimensionless ground-state energy per particle with the difference in the noninteracting kinetic energy for a finite and infinite system (top) and the number of particles (bottom) for various interaction parameters $\eta = \ln(k_F a)$ in the zero effective-range limit $k_F^2 R_{\rm eff}^2 = 0$. The straight lines show a weighted least-squares fit to the data points.

### 2. System size extrapolation

Our quantum Monte Carlo algorithm simulates a finite number of particles $N$, placed at discrete momentum vectors. This introduces a systematic error in the kinetic energy, which in two dimensions is proportional to $(1/N)^{\frac{5}{4}}$ [62]. The bias is corrected by performing simulations with varying particle number and extrapolating $N \to \infty$ by fitting the energy per particle of the $N$-particle system, $E_N$, to the formula [48],

$$E_N = E_\infty + a(T_N - T_\infty) + bT_\infty/N,$$

where $E_\infty$ is the energy per particle for an infinite system, $T_N$ is the kinetic energy of a noninteracting $N$-particle system, the coefficient $a$ captures the rapid oscillations from the discreteness of the wave vectors, while $b$ captures residual finite-size effects that are expected to fade away as $N \to \infty$, and $T_\infty = \frac{1}{2}E_F$.

We perform simulations with $N = \{26,42,58,98\}$ particles, and the procedure is illustrated for $k_F^2 R_{\rm eff}^2 = 0$ and several values of the interaction parameter $\eta = \ln(k_F a)$ in Fig. 12. With simulations at four different number of particles, the predicted error in the extrapolate includes both statistical and systematic contributions. As shown in the top graph, oscillations are large in the weakly interacting BCS regime, corresponding to large values of $\eta$, where the ground-state wave function is close to that of the noninteracting system and the variation in the dimensionless ground-state energy is up to 0.09 over

the range of particle numbers studied. As the value of $\eta$ is reduced, the interparticle interaction becomes stronger and we approach the BEC regime consisting of tightly bound fermion pairs, washing out the finite-size effects for $\eta \leqslant 0$.

As demonstrated in the bottom graph, the residual finite-size effects are an order of magnitude smaller with a maximum variation in the dimensionless ground-state energy of only $6\times10^{-3}$. We conclude that finite-size extrapolations are essential to achieve a target accuracy for the dimensionless ground-state energy of $10^{-3}$, particularly in the BCS regime where oscillations in the kinetic energy lead to finite-size errors up to $5\times10^{-2}$.


[1] Y.-J. Lin, R. L. Compton, K. Jiménez-García, J. V. Porto, and I. B. Spielman, Nature (London) **462**, 628 (2009).
[2] Z. Hadzibabic, P. Krüger, M. Cheneau, B. Battelier, and J. Dalibard, Nature (London) **441**, 1118 (2006).
[3] P. A. Lee, N. Nagaosa, and X.-G. Wen, Rev. Mod. Phys. **78**, 17 (2006).
[4] K. Martiyanov, V. Makhalov, and A. Turlapov, Phys. Rev. Lett. **105**, 030404 (2010).
[5] A. Görlitz, J. M. Vogels, A. E. Leanhardt, C. Raman, T. L. Gustavson, J. R. Abo-Shaeer, A. P. Chikkatur, S. Gupta, S. Inouye, T. Rosenband, and W. Ketterle, Phys. Rev. Lett. **87**, 130402 (2001).
[6] C. Chin, R. Grimm, P. Julienne, and E. Tiesinga, Rev. Mod. Phys. **82**, 1225 (2010).
[7] I. Bloch, J. Dalibard, and W. Zwerger, Rev. Mod. Phys. **80**, 885 (2008).
[8] A. T. Sommer, L. W. Cheuk, M. J. H. Ku, W. S. Bakr, and M. W. Zwierlein, Phys. Rev. Lett. **108**, 045302 (2012).
[9] K. Günter, T. Stöferle, H. Moritz, M. Köhl, and T. Esslinger, Phys. Rev. Lett. **95**, 230401 (2005).
[10] J.-P. Martikainen and P. Törmä, Phys. Rev. Lett. **95**, 170407 (2005).
[11] A. A. Orel, P. Dyke, M. Delehaye, C. J. Vale, and H. Hu, New J. Phys. **13**, 113032 (2011).
[12] I. Boettcher, L. Bayha, D. Kedar, P. A. Murthy, M. Neidig, M. G. Ries, A. N. Wenz, G. Zürn, S. Jochim, and T. Enss, Phys. Rev. Lett. **116**, 045303 (2016).
[13] D. S. Petrov, M. A. Baranov, and G. V. Shlyapnikov, Phys. Rev. A **67**, 031601 (2003).
[14] S. S. Botelho and C. A. R. Sá de Melo, Phys. Rev. Lett. **96**, 040404 (2006).
[15] W. Zhang, G.-D. Lin, and L.-M. Duan, Phys. Rev. A **78**, 043617 (2008).
[16] G. J. Conduit, P. H. Conlon, and B. D. Simons, Phys. Rev. A **77**, 053617 (2008).
[17] V. Ngampruetikorn, J. Levinsen, and M. M. Parish, Phys. Rev. Lett. **111**, 265301 (2013).
[18] N. D. Drummond, N. R. Cooper, R. J. Needs, and G. V. Shlyapnikov, Phys. Rev. B **83**, 195429 (2011).
[19] B. J. Verhaar, J. P. H. W. van den Eijnde, M. A. J. Voermans, and M. M. J. Schaffrath, J. Phys. A: Math. Gen. **17**, 595 (1984).
[20] S. K. Adhikari, W. G. Gibson, and T. K. Lim, J. Chem. Phys. **85**, 5580 (1986).
[21] G. Bertaina and S. Giorgini, Phys. Rev. Lett. **106**, 110403 (2011).
[22] H. Shi, S. Chiesa, and S. Zhang, Phys. Rev. A **92**, 033603 (2015).
[23] A. Galea, H. Dawkins, S. Gandolfi, and A. Gezerlis, Phys. Rev. A **93**, 023602 (2016).
[24] Y. Wang, J. P. D'Incao, and B. D. Esry, Phys. Rev. A **83**, 042710 (2011).
[25] M. Randeria, J.-M. Duan, and L.-Y. Shieh, Phys. Rev. Lett. **62**, 981 (1989).
[26] M. Randeria, J.-M. Duan, and L.-Y. Shieh, Phys. Rev. B **41**, 327 (1990).
[27] C. W. von Keyserlingk and G. J. Conduit, Phys. Rev. B **87**, 184424 (2013).
[28] P. O. Bugnion, P. L. Ríos, R. J. Needs, and G. J. Conduit, Phys. Rev. A **90**, 033626 (2014).
[29] T. M. Whitehead, L. M. Schonenberg, N. Kongsuwan, R. J. Needs, and G. J. Conduit, Phys. Rev. A **93**, 042702 (2016).
[30] L. M. Schonenberg and G. J. Conduit, Phys. Rev. A **95**, 013633 (2017).
[31] V. Gurarie and L. Radzihovsky, Ann. Phys. (NY) **322**, 2 (2007).
[32] E. Timmermans, T. Tomassini, M. Hussein, and A. Kerman, Phys. Rep. **315**, 199 (1999).
[33] S. K. Adhikari, Am. J. Phys. **54**, 362 (1986).
[34] D. S. Petrov and G. V. Shlyapnikov, Phys. Rev. A **64**, 012706 (2001).
[35] Some authors use an alternative definition of the scattering length, $a' = 2ae^{-\gamma}$ with $\gamma \approx 0.577$ Euler's constant. In this case $E_b = -e^{2\gamma}/4ma'^2$ .
[36] D. Bollé, F. Gesztesy, C. Danneels, and S. F. J. Wilk, Phys. Rev. Lett. **56**, 900 (1986).
[37] For the existence of the bound the mean-field definition of attractive, i.e., $\int V(\mathbf{r})d\mathbf{r} < 0$, is sufficient, which automatically includes all potentials satisfying the more stringent condition of uniform attractiveness, $V(\mathbf{r}) < 0$.
[38] C. A. Kocher, Am. J. Phys. **45**, 71 (1977).
[39] F. Coutinho, C. Malta, and J. F. Perez, Phys. Lett. A **97**, 242 (1983).
[40] J. H. Lloyd-Williams, R. J. Needs, and G. J. Conduit, Phys. Rev. B **92**, 075106 (2015).
[41] T. M. Whitehead and G. J. Conduit, Phys. Rev. A **93**, 022706 (2016).
[42] G. E. Astrakharchik, J. Boronat, J. Casulleras, and S. Giorgini, Phys. Rev. Lett. **93**, 200404 (2004).
[43] G. E. Astrakharchik, J. Boronat, J. Casulleras, and S. Giorgini, Phys. Rev. Lett. **95**, 230405 (2005).
[44] M. M. Forbes, S. Gandolfi, and A. Gezerlis, Phys. Rev. A **86**, 053603 (2012).
[45] R. J. Needs, M. D. Towler, N. D. Drummond, and P. L. Ríos, J. Phys.: Condens. Matter **22**, 023201 (2010).
[46] D. M. Ceperley and B. J. Alder, Phys. Rev. Lett. **45**, 566 (1980).
[47] C. J. Umrigar, M. P. Nightingale, and K. J. Runge, J. Chem. Phys. **99**, 2865 (1993).
[48] W. M. C. Foulkes, L. Mitas, R. J. Needs, and G. Rajagopal, Rev. Mod. Phys. **73**, 33 (2001).
[49] P. L. Ríos, A. Ma, N. D. Drummond, M. D. Towler, and R. J. Needs, Phys. Rev. E **74**, 066701 (2006).
[50] M. Mella, G. Morosi, and D. Bressanini, Phys. Rev. E **61**, 2050 (2000).
[51] A. Sarsa, J. Boronat, and J. Casulleras, J. Chem. Phys. **116**, 5956 (2002).

[52] Note that although Ceperley and Kalos [53] report that the extrapolated estimate works in practice for matrix elements off diagonal in position space, such as the momentum distribution and condensate fraction, their formal derivation breaks down for nonlocal operators.
[53] D. M. Ceperley and M. H. Kalos, in *Monte Carlo Methods in Statistical Physics*, 2nd ed., edited by K. Binder (Springer, Berlin, 1986), Chap. 4, pp. 145–194.
[54] M. P. Nightingale and C. J. Umrigar, in *Quantum Monte Carlo Methods in Physics and Chemistry* (Springer Science & Business Media, Berlin, 1998), Chap. 1, pp. 1–36.
[55] S. Tan, Ann. Phys. (NY) **323**, 2971 (2008); **323**, 2987 (2008); **323**, 2952 (2008).
[56] M. Schick, Phys. Rev. A **3**, 1067 (1971).
[57] L. Salasnich, Phys. Rev. A **76**, 015601 (2007).
[58] A. J. Leggett, *Quantum Liquids: Bose Condensation and Cooper Pairing in Condensed-Matter Systems* (Oxford University Press, Oxford, 2006).
[59] E. Braaten, D. Kang, and L. Platter, Phys. Rev. A **78**, 053606 (2008).
[60] L. M. Schonenberg, G. J. Conduit, and P. C. Verpoort, The data repository has now been made available and can be found under the following doi: 10.17863/CAM.7092.
[61] R. M. Lee, G. J. Conduit, N. Nemec, P. L. Ríos, and N. D. Drummond, Phys. Rev. E **83**, 066706 (2011).
[62] N. D. Drummond, R. J. Needs, A. Sorouri, and W. M. C. Foulkes, Phys. Rev. B **78**, 125106 (2008).